Search for a TeV Component of Gamma-Ray Bursts Using the Milagrito Detector

R. Atkins,[1] W. Benbow,[2] D. Berley,[3,4] M.-L. Chen,[3,11] D. G. Coyne,[2] B. L. Dingus,[1] D. E. Dorfan,[2] R. W. Ellsworth,[5] D. Evans,[3] A. Falcone,[6] L. Fleysher,[7] R. Fleysher,[7] G. Gisler,[8] J. A. Goodman,[3] T. J. Haines,[8] C. M. Hoffman,[8] S. Hugenberger,[9] L. A. Kelley,[2] I. R. Leonor,[9] M. McConnell,[6] J. F. McCullough,[2] J. E. McEnery,[1] R. S. Miller,[6,8] A. I. Mincer,[7] M. F. Morales,[2] P. Nemethy,[7] J. M. Ryan,[6] B. Shen,[10] A. Shoup,[9] C. Sinnis,[8] A. J. Smith,[3,10] G. W. Sullivan,[3] T. Tumer,[10] K. Wang,[10,12] M. O. Wascko,[10,13] S. Westerhoff,[2,14] D. A. Williams,[2] T. Yang,[2] and G. B. Yodh[9]

(The Milagro Collaboration)

---

[1]University of Wisconsin, Madison, WI 53706.

[2]University of California, Santa Cruz, Santa Cruz, CA 95064.

[3]University of Maryland, College Park, MD 20742.

[4]Permanent address: National Science Foundation, Arlington, VA 22230.

[5]George Mason University, Fairfax, VA 22030.

[6]University of New Hampshire, Durham, NH 03824.

[7]New York University, New York, NY 10003.

[8]Los Alamos National Laboratory, Los Alamos, NM 87545.

[9]University of California, Irvine, Irvine, CA 92697.

[10]University of California, Riverside, Riverside, CA 92521.

[11]Now at Brookhaven National Laboratory, Upton, NY 11973.

[12]Now at Fresher Information Corp., San Francisco, CA 94105.

[13]Now at Louisiana State University, Baton Rouge, LA 70803.

[14]Now at Columbia University, New York, NY 10027.

ABSTRACT

The past decade has seen an explosion in our understanding of gamma-ray bursts (GRBs). Due mainly to recent progress made in the fast and precise localizations of GRBs, multiwavelength studies of these astrophysical objects are now a reality. These studies at radio, optical, x-ray, and keV-MeV gamma-ray wavelengths, have led to a good, though incomplete, understanding of the distance scale to GRBs, their energetics, and the physical processes which give rise to the radiation which is eventually detected on Earth. This paper presents the results of work undertaken to contribute to current multiwavelength efforts at understanding GRBs by observing these astrophysical objects in the TeV energy regime using Milagrito, a water Cherenkov extensive air shower array which was sensitive to TeV gamma-rays and which was well-suited for catching a glimpse of these ephemeral objects. The search was made by examining 54 BATSE GRBs for TeV emission which was coincident with emission in the keV-MeV regime. The search revealed that one of the GRBs examined, GRB 970417a, was a candidate TeV GRB. Implications of a TeV detection on the GRB distance scale and energetics are discussed. Upper limits on GRB flux at TeV energies for the other GRBs examined are also given.

Subject headings: gamma rays: bursts – gamma rays: observations

1. Introduction

Today, it is known that the astrophysical phenomenon denominated as gamma-ray bursts (GRBs) is capable of giving rise to electromagnetic radiation from radio wavelengths to gamma-ray wavelengths. These cosmic objects were previously only seen as brief and intense flashes of keV-MeV radiation, lasting anywhere from a fraction of a second to some hundreds of seconds, with most of the energy being in the form of $\sim$ 200-keV photons, hence their appellation. In 1997, however, the rapid and precise localization of GRB 970228 by BeppoSAX (Costa et. al. 1997) enabled follow-up observations of this GRB by other astronomical instruments and, for the first time, made possible the detection of long-lived, rapidly decaying optical and x-ray afterglows from a GRB (Costa et. al. 1997; van Paradijs et. al. 1997; Bloom, Djorgovski, & Kulkarni 2000a). At present, fast and precise localizations of GRBs by the satellite missions BeppoSAX (Boella et. al. 1997), RXTE (Levine et. al. 1996; Bradt & Smith 1999), and the Third Interplanetary Network (IPN3) (Hurley 1999), have made possible routine follow-up observations of GRBs for multiwavelength afterglows by ground-based and satellite-based astronomical instruments. About half of the GRBs examined for afterglow emission have one or more long-lived counterparts at x-ray, optical, or radio wavelengths (Greiner 2000).

Detections of optical counterparts to some GRBs have provided opportunities to directly measure the distances to more than a dozen of these GRBs through spectroscopic redshift measurements. The median redshift of this sample of GRBs is $z \approx 1$. The measured gamma-ray fluences and redshifts for these bursts, thus, imply an isotropic energy release of $\sim 10^{51}$ to $\sim 10^{54}$ $ergs$ during the GRBs' short lifetimes. Table 1 lists GRBs with a measured or estimated redshift.

The observed general characteristics of GRBs, i.e. their nonthermal spectra, the highly variable temporal features found in most GRB light curves, as well as the afterglow phenomenon, are well accounted for by the relativistic fireball model of GRBs, also called the internal-external shocks model (see, for example, Piran (1999, 2000)). In this GRB model, an inner engine gives rise to a radiation-plasma fireball. Eventually, subsequent to the relativistic expansion of the fireball, most of the initial fireball energy is converted into bulk kinetic energy of baryonic matter which may have been ejected together with the fireball, with the baryonic matter attaining an ultrarelativistic velocity corresponding to a bulk relativistic Lorentz factor, $\Gamma > 100$. The engine activity could be highly variable, giving rise to multiple fireballs and highly variable particle winds, and thus to multiple shells of matter with different Lorentz factors. When a fast shell catches up with a slow shell, the two shells

Table 1. GRBs with a measured or estimated redshift.

GRB	Burst[a] Duration (*seconds*)	Fluence in[b] Gamma-rays ($ergs\ cm^{-2}$)	z[c]	Implied[d] Isotropic Energy Release (*ergs*)	References (with useful references therein)
970228	80	1.1×10^{-5}	0.6950 ± 0.0003	1.0×10^{52}	1, 2
970508	23	3.1×10^{-6}	0.8349 ± 0.0003	4.0×10^{51}	3, 4, 5, 6, 7
971214	31	1.1×10^{-5}	3.418 ± 0.010	1.4×10^{53}	3, 8
980326	5	1.4×10^{-6}	≈ 1[e]	2.4×10^{51}	9, 10
980425	23	4.4×10^{-6}	0.0085 ± 0.0002	8.1×10^{47}	11, 12, 13
980613	20	1.7×10^{-6}	1.0969 ± 0.0002	3.5×10^{51}	14, 15
980703	412	4.6×10^{-5}	0.9662 ± 0.0002	7.6×10^{52}	3, 16, 17
990123	63	5.1×10^{-4}	1.6004 ± 0.0008	2.0×10^{54}	3, 18
990510	68	2.3×10^{-5}	1.619 ± 0.002	9.0×10^{52}	3, 19
990705	42	$\sim 9 \times 10^{-5}$	0.86[f]	1.2×10^{53}	20
990712	30	···	0.4337 ± 0.0004	···	21, 22
991208	68	$\sim 10^{-4}$	0.707 ± 0.002	9.6×10^{52}	23, 24
991216	15	2.6×10^{-4}	1.02	4.7×10^{53}	3, 25
000131	96	3.5×10^{-5}	4.500 ± 0.015	6.5×10^{53}	26
000214	10	1.4×10^{-5}	0.47[g]	6.4×10^{51}	27
000301c	2	$\sim 4 \times 10^{-6}$	2.0404 ± 0.0008	2.3×10^{52}	28
000418	30	1.3×10^{-5}	1.11854 ± 0.0007	2.8×10^{52}	29, 30
000926	25	2.2×10^{-5}	2.0369 ± 0.0007	1.2×10^{53}	31, 32, 33
010222	130	9.2×10^{-5}	1.477	3.1×10^{53}	34, 35

[a]Duration of gamma-rays measured by one of the following satellite experiments: BATSE, Ulysses, NEAR, or GRBM on board BeppoSAX.

[b]Fluence in gamma-rays measured by one of the satellite experiments mentioned above.

[c]Measured or estimated redshift. Unless otherwise stated, measured redshifts are either from observed emission lines from the host galaxy, or from observed absorption lines from the optical transient.

[d]Calculated assuming a flat, Einstein-de Sitter Universe ($\Omega = 1$, $\Lambda = 0$), and $H_o = 65\ km\ s^{-1}\ Mpc^{-1}$.

[e]Estimated from model fits to the observed optical light curve assuming an underlying supernova.

[f]Estimated using the absorption edge found in the prompt x-ray spectrum.

[g]Estimated using the iron $K\alpha$ line found in the x-ray afterglow.

References. — (1) Costa et. al. (1997); (2) Bloom, Djorgovski, & Kulkarni (2000a); (3) BATSE Catalog (2000); (4) Galama et. al. (1998a); (5) Metzger et. al. (1997a); (6) Metzger et. al. (1997b); (7) Bloom et. al. (1998); (8) Kulkarni et. al. (1998a); (9) Groot et. al. (1998); (10) Bloom et. al. (1999a); (11) Galama et. al. (1998b); (12) Iwamoto et. al. (1998); (13) Kulkarni et. al. (1998b); (14) Djorgovski, Bloom, & Kulkarni (2000); (15) Woods et. al. (1998); (16) Vreeswijk et. al. (1999); (17) Djorgovski et. al. (1998); (18) Kulkarni et. al. (1999); (19) Wijers et. al. (1999); (20) Amati et. al. (2000); (21) Sahu et. al. (2000); (22) Hjorth et. al. (2000); (23) Hurley et. al. (2000a); (24) Dodonov et. al. (1999); (25) Halpern et. al. (2000); (26) Andersen et. al. (2000); (27) Antonelli et. al. (2000); (28) Jensen et. al. (2001); (29) Klose et. al. (2000); (30) Bloom et. al. (2000b); (31) Hurley et. al. (2000b); (32) Hurley et. al. (2000c); (33) Castro et. al. (2000); (34) Jha et. al. (2001); (35) in 't Zand et. al. (2001).

collide inelastically, forming a shock wherein electrons coupled to the baryonic matter are accelerated. The shock acceleration of these electrons in an ambient magnetic field effects the production of synchrotron radiation which is detected on Earth as the main gamma-ray burst. In this model, the observed duration of the gamma-ray burst corresponds to the duration of the engine activity, while the observed temporal variability in the GRB light curves reflects the highly variable nature of the engine activity. The subsequent expansion of the relativistic shells of matter into an ambient medium of low-density gas, which could be an interstellar medium or stellar wind associated with the GRB progenitor, causes the slowing down of the shells and the production of external shocks, which again leads to the acceleration of electrons and to the production of synchrotron radiation, this time at longer wavelengths than those produced in the internal shocks. This radiation is what is observed as GRB afterglow at x-ray, optical, or radio wavelengths.

The physical process which powers a GRB is popularly believed to be the accretion of matter into a black hole. Popular models for the production of such an inner engine can be generally classified into two: Stellar remnant merger models (Piran 1999, 2000; Bloom, Sigurdsson, & Pols 1999b; Rosswog et. al. 1999; Ruffert & Janka 1999) and stellar collapse models (Woosley 1993; Paczyński 1998; Woosley & MacFadyen 1999; MacFadyen & Woosley 1999). Stellar remnant merger models basically involve a binary system of stellar remnants orbiting each other which, due to emission of gravitational radiation, eventually loses rotational energy, causing the dead stars to spiral into each other and collide, forming a black hole-accretion disk system. Falling in this category are neutron star-neutron star mergers, and neutron star-black hole mergers. Stellar collapse models, on the other hand, involve the collapse of the iron core of a massive, rotating star which is at the end of its evolution. The collapse of the iron core would lead to the production of a black hole into which the star's outer layers would accrete. In this model, the generation of a supernova is also possible. Stellar collapse models go by the names collapsar or failed Type Ib/c supernova, and hypernova. A variant scenario is the supranova model (Vietri & Stella 1998), in which the black hole is formed in a two-step process through a supernova explosion, and then the subsequent collapse of the created supramassive neutron star as it loses angular momentum. Since these GRB progenitor models involve massive stars, it has been suggested that GRBs trace the star formation history of the Universe (Lamb 2000; Wijers et. al. 1998; Lamb & Reichart 2000; Hogg & Fruchter 1999; Totani 1999).

In the context of the relativistic fireball model of GRBs, it is possible to produce TeV photons, as observed on Earth, through the inverse Compton scattering of the synchrotron radiation produced in internal shocks off the shock-accelerated electrons. The emergence of such a TeV component is expected to be prompt, coincident with the synchrotron radiation seen in the keV-MeV waveband (Pilla & Loeb 1998; Piran 1999). This synchrotron self-Compton (SSC) mechanism is widely believed to be the physical process which is responsible for TeV emission observed from a few well-known astrophysical TeV sources, i.e. the Crab nebula (Aharonian et. al. 2000; Hillas et. al. 1998; Tanimori et. al. 1998; de Jager et. al. 1996; de Jager & Harding 1992), and the BL Lacartae Markarian 421 and Markarian 501 (Takahashi et. al. 2000; Maraschi et. al. 1999; Krennrich et. al. 1999; Zweerink et. al. 1997; Krennrich et. al. 1997; Petry et. al. 2000; Aharonian et. al. 1999a,b; Quinn et. al. 1999; Samuelson et. al. 1998; Inoue & Takahara 1996; Bloom & Marscher 1996). The observed energy spectra of these sources span a wide range of energies, from radio to TeV energies. The low-energy emission is believed to be due to synchrotron radiation from relativistic electrons accelerated in the astrophysical sources, while the high-energy emission is thought to be due to the inverse Compton scattering of the synchrotron photons off the same population of relativistic electrons.

There have been searches made for TeV emission from GRBs by various extensive air shower (EAS) arrays and air Cherenkov telescopes (Padilla et. al. 1998; Amenomori et. al.

1996; Connaughton et. al. 1997; Aglietta et. al. 1996; Alexandreas et. al. 1994). Two of these searches have resulted in tentative evidence for TeV emission (Padilla et. al. 1998; Amenomori et. al. 1996), but none have resulted in convincing evidence for such emission. This paper presents the results of another search for TeV emission from GRBs using the Milagrito detector, a ground-based water Cherenkov air shower array which, as will be evident in the next section, is endowed with characteristics which give it advantages over traditional EAS arrays, as well as air Cherenkov telescopes, when it comes to searching for TeV transients. Additionally, the results of a search for TeV GRBs using Milagrito which is completely independent of the work presented here can be found in Atkins et. al. (2000a).

2. The Milagrito Detector

Milagrito was the first functional detector of extensive air showers in the TeV regime which utilized the water Cherenkov technique. The detector and its performance are described in detail in Atkins et. al. (2000b). In contrast to traditional EAS arrays, which generally make use of a sparse distribution of discrete scintillation detectors covered with an optimal thickness of lead to convert air shower electrons and photons into visible light which could be detected by photomultiplier tubes (PMTs), Milagrito made use of water as the single medium with which both the electron and photon components of an air shower could interact to subsequently produce Cherenkov light. In this type of detector, the combination of using a continuous medium to ultimately produce light from the transit of air shower particles, and the large emission angle of Cherenkov light in water ($\approx 42°$), ensures an efficient sampling of air shower particles by the detector, even if a sparse array of PMTs is used to detect the Cherenkov light. Thus, small showers which could not be detected by traditional scintillation EAS arrays could be detected by a water Cherenkov detector, resulting in a lower energy threshold. At small zenith angles ($< 25°$) and using a 100-tube trigger requirement, Milagrito had an energy threshold of $\sim 300\ GeV$, comparable to the energy threshold of some air Cherenkov telescopes.

Milagrito was located in the Jemez Mountains of New Mexico, in the complex of what is now known as the Fenton Hill Observatory. It's elevation was 2646 meters, which translates to an atmospheric overburden of 750 $g\ cm^{-2}$, or about 20 radiation lengths. It was in operation for 15 months, from February 1997 to May 1998. The water reservoir which housed the main part of the experiment had a trapezoidal shape, with a bottom which was 50 meters long by 30 meters wide, an aperture at the top which was 80 meters long by 60 meters wide, a depth of 8 meters, and sloping sides. There were a total of 228 20.3-cm diameter PMTs deployed, arranged into 12 columns and 19 rows, anchored near the bottom of the pond. The distance between adjacent PMTs was 2.8 meters. Since each encapsulated PMT had a buoyancy of about 10 pounds (44.5 N) and was bottom heavy, each PMT floated to an upright position, with the photocathode facing upward, with the addition of water to the reservoir.

During most of Milagrito's lifetime, the water level in the pond was such that there was ≈ 1 meter of water above the PMTs' photocathodes. During the latter part of the detector's life, the water level was increased so that there was, first 1.5 meters, then 2.0 meters of water above the PMTs. Since the purpose of the PMTs was to detect Cherenkov light produced by air shower particles traversing the water, it was necessary to make the pond lighttight to prevent any extraneous light from being detected by the PMTs. This was accomplished by covering the pond with a 1-mm thick black material made of two layers of polypropylene with an internal layer of polyester scrim.

The design of the Milagrito detector as described above, i.e. the use of the water Cherenkov technique, the wide aperture, and the lighttight cover, grants this experiment characteristics which are desirable in the task of observing fugitive astrophysical TeV sources:

a low energy threshold, a wide field of view, and the ability to continuously monitor the sky during both daytime and nighttime. Milagrito was, thus, well-suited for the work of searching for a TeV component of GRBs.

The arrival direction of a primary particle incident at the top of the atmosphere, and which seeded a detectable extensive air shower, was reconstructed by using the relative times of arrival of Cherenkov light at the PMTs. After correcting the raw arrival times for shower curvature and pulse height dependence, and applying PMT calibration parameters, the corrected arrival times were used in a chi-square minimization algorithm to reconstruct a planar shower front and to estimate the zenith angle and azimuth angle of the primary particle. This reconstruction algorithm resulted in an angular resolution of $\approx 1\overset{\circ}{.}4$, on the average. The quality of the angular resolution was limited in part by the inability of the reconstruction algorithm to estimate the locations of shower cores, especially those which landed outside the pond, with good accuracy. This shortcoming was a direct consequence of the fact that the physical size of Milagrito was much smaller than the size of air showers, at Milagrito's altitude, initiated by TeV primaries, so that extensive air showers which were large enough in lateral extent could still trigger Milagrito even when their cores landed considerably far from the water pond. The inability to accurately determine the shower core location also made it very difficult to estimate the size of an air shower and, therefore, the energy of the initiating primary particle.

3. Data Analysis Technique

The search for a TeV component of GRBs was conducted by examining GRBs which were seen by the Burst and Transient Source Experiment (BATSE) (Fishman 1992; BATSE Catalog 2000; Pendleton et. al. 1999) in the soft keV-MeV gamma-ray waveband. During Milagrito's lifetime, there were 54 such BATSE GRBs whose best positions, as measured by

BATSE, were within 45° of Milagrito's zenith, and it was this sample of GRBs which was used in this work. The search was limited to GRBs with small nominal zenith angles because increasing atmospheric overburden at increasing zenith angles translated to less Milagrito sensitivity at large zenith angles, assuming a falling source TeV energy spectrum at the top of the atmosphere. Since there was a large uncertainty, of the order of a few degrees, in each of the measured BATSE GRB positions considered, the patch of celestial sphere which was examined for TeV emission was a GRB's 95% confidence area as determined by BATSE (Briggs et. al. 1999). The radii of the 54 search areas used in this analysis ranged from $\approx 6°$ to $\approx 30°$.

Each GRB search area, centered at the best declination and right ascension coordinates determined by BATSE, was systematically examined for TeV emission by first dividing the area into a grid of non-overlapping, square celestial bins (see Fig. 1), then determining if there was a significant excess in the number of events reconstructed as coming from the bins during the BATSE T90 duration for that GRB. The BATSE T90 duration is defined as the time interval during which 90% of the total gamma-ray event count for a GRB were detected. For the sample of 54 GRBs, the BATSE T90 durations ranged from ≈ 0.2 second to ≈ 200 seconds. The size of the bins used for a particular search area depended on Milagrito's angular resolution, and on the average expected background in the search area at the time of the burst. Generally, the larger the zenith angle of the search area at the time of the burst, the smaller the average expected background, and the larger the bin size used in the search. The general idea was, if the expected background count was small, the bin could be made larger to be more efficient at encompassing possible signal events. To be efficient at detecting potential sources which lay near bin edges, the search technique also involved shifting the search grid half a bin width in declination, then half a bin width in right ascension, then half a bin width in both directions, and performing a search at each of these grid configurations. Since using several bins meant that there were several trials used in the search, care was also

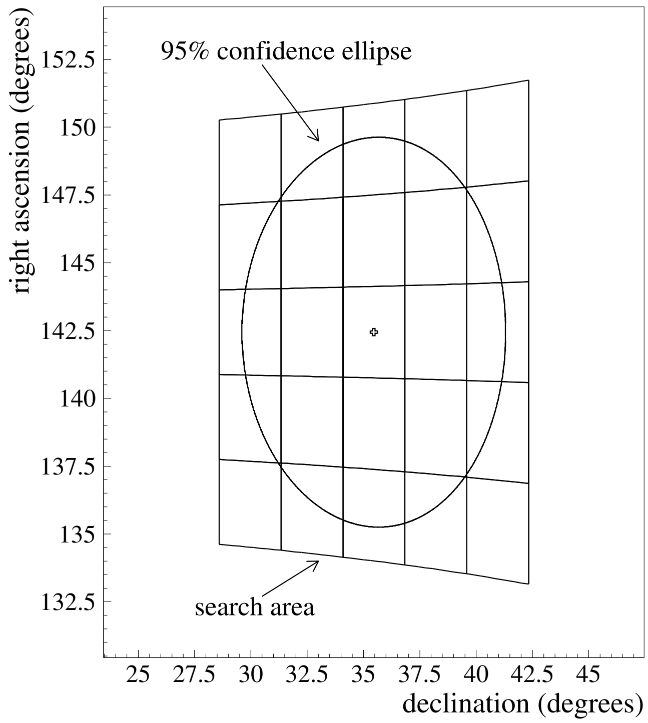

Fig. 1.— Search area and bin configuration used for one of the GRBs examined. The nominal GRB position given in the current BATSE catalog is at the center of the plot.

taken not to make the bin sizes so small as to increase the number of trials considerably. The bin sizes which were optimal for this type of search were determined through computer simulations. The bin widths used in the different search areas ranged from $2^\circ\!.4$ to $3^\circ\!.9$ in declination, and $2^\circ\!.4/cos(\delta)$ to $3^\circ\!.9/cos(\delta)$ in right ascension, where δ was the declination of the center of a bin in a search area.

For each GRB search area, the expected background count in each of the bins during T90 was calculated using,

$$N_b(\theta,\phi,t) = \frac{N_{off}(\theta,\phi)}{N_{tot}} \begin{cases} R(t)T90 & \text{if T90} < 10 \text{ seconds} \quad , \\ N_{T90}(t) & \text{if T90} > 10 \text{ seconds} \quad ; \end{cases} \tag{1}$$

where (θ,ϕ) were the corresponding local zenith and azimuth angles of the center of the bin at the middle of the T90 interval, t; $N_{off}(\theta,\phi)$ is called the off-source count and was the number of background events falling into the local (θ,ϕ) bin during a six-hour time interval centered at T90, N_{tot} was the total number of background events detected from the entire sky during the same six-hour period, $R(t)$ was the measured average all-sky event rate during a two-minute time interval centered at the middle of the T90 interval, and N_{T90} was the all-sky background event count during T90. In this procedure, the motion of the celestial sphere relative to the local sky during T90 was ignored, an approximation which is valid in the limit of short time intervals. Once the expected background count during T90 in a bin in a search area was estimated, the actual number of events falling in the bin during T90, called the on-source count, could be compared to this expected background count to ascertain if there was a significant event excess in that bin.

4. Results of Search for a TeV Component of GRBs

Figure 2a is the distribution of the significance of the most significant measured excess from each GRB search area. The calculation of significance in this case follows the prescription of Li & Ma (1983). Figure 2b gives the distribution of the cumulative Poisson probability for the occurrence of the measured on-source count or larger in the most significant bin from each GRB search area, given the expected background count in that bin. It can be seen from the distributions that one GRB search area, that of GRB 970417a (BATSE trigger number 6188), gave rise to a bin which had an excess with a pre-trials significance of 5.2 standard deviations. For the search time interval of 7.9 seconds for this GRB, this particular bin had an on-source count of 17 events, and an estimated background of 3.41 ± 0.04 events. This means that the cumulative Poisson probability for the occurrence of the on-source count or larger given the estimated background is 1.3×10^{-7}. More details about the analysis of GRB 970417a's search area is found in Section 5.

If there was a single trial used for each GRB area search, the significances and probabilities given in Fig. 2 would be sufficient to assess the most significant excess found in each search area. Because there were several bins used in each search area, amounting to several trials per search area, it was necessary to determine the probability for the occurrence of the most significant excess from a search area due to background fluctuations, given the number of trials used in that search area. This post-trials probability was determined for each search area by scanning the Milagrito data and calculating the fraction of times that an excess with a significance at least as large as the largest significance found in the real search is measured, using the same search technique and search configuration, i.e. the same search duration, the same search area size, the same grid and bin geometry, the same local area of the sky, as that used in the real search. The integral distribution of post-trials probabilities for the most significant excesses from the 54 search configurations is plotted in Fig. 3. For a particular post-trials probability, Fig. 3 plots the number of GRB search configurations which gave rise to that probability or less, e.g. there were 54 GRB search configurations which had a post-trials probability of 1 or less. Figure 3 also shows the expected distribution if there were no TeV sources in the 54 search areas, i.e. if the most significant excesses found were due

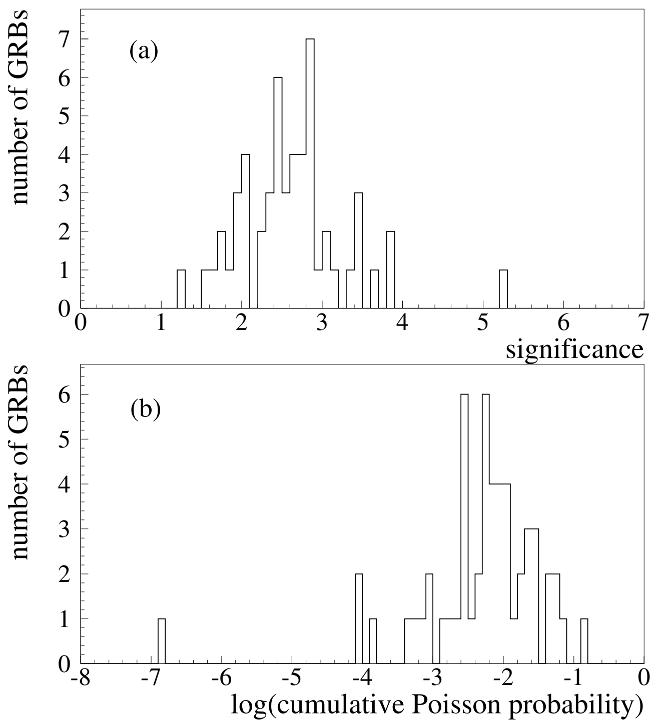

Fig. 2.— (a) Distribution of significance of the most significant excess from each GRB search area. (b) Distribution of cumulative Poisson probability for the occurrence of the measured on-source count or larger in the most significant bin from each GRB search area given the estimated background in that bin.

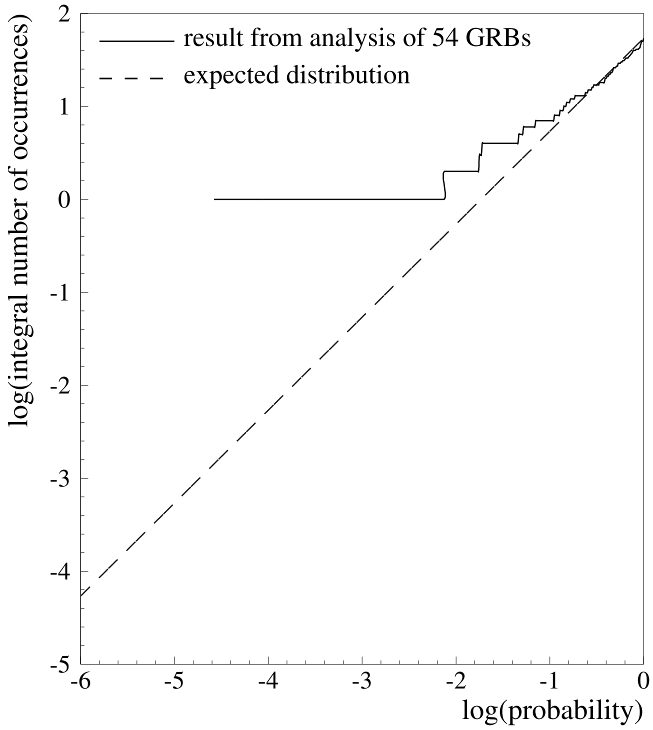

Fig. 3.— Integral distribution of post-trials probabilities.

to background fluctuations only. The expected distribution in Fig. 3 has a slope of 1.0 and corresponds to a flat distribution of probabilities in a differential plot with linear scales. It can be seen that the tail of the actual distribution deviates from the expected distribution.

The post-trials probability for the most significant excess found in GRB 970417a's search area is 2.6×10^{-5}, or a significance of 4.2 standard deviations. It can be seen from the expected distribution in Fig. 3 that, if $n(\leq p)$ is the number of GRB search configurations which would be expected to give rise to a post-trials probability of p or less, the probability of occurrence from a search configuration of a post-trials probability p or less due to background fluctuations is $n(\leq p)/54 = p$, regardless of which search configuration is considered. Since there were 54 search configurations considered, the final probability for getting a post-trials probability of p or less in at least one search configuration is given by the binomial distribution,

$$P_f(\leq p) = 1 - (1-p)^{54} \quad . \tag{2}$$

Thus, the most significant excess found in GRB 970417a's search area, for which $p = 2.6 \times 10^{-5}$, has a final probability of 1.4×10^{-3}, or a significance of 3.2 standard deviations. In other words, one in 700 analyses of 54 search configurations will give rise to at least one occurrence of a post-trials significance of 4.2 or larger due to background fluctuations.

Upper limits on the GRB flux at TeV energies have been set at the 90% confidence level for most of the GRBs for which no meaningful excesses were found. For the calculation of flux upper limits, the model assumed for the GRB differential energy spectrum at the top of the atmosphere at TeV energies, in units of number of photons per unit area per unit time per unit energy, was a power law, i.e.

$$\frac{dF}{dE} = F_o E^{-\eta} \quad , \tag{3}$$

where F_o is a normalization constant, η is the differential spectral index, both assumed to be constant with time, and E is photon energy in TeV. For each bin with an excess in a GRB search area, a 90% upper limit on the flux normalization was set by using the measured on-source count and estimated background for that bin during T90 to calculate a 90% upper limit on the possible number of signal events, N_{90}. N_{90} and the corresponding 90% upper limit on the flux normalization, F_o, are related by,

$$N_{90}(\theta,\phi) = \epsilon \Delta T F_o(\theta,\phi) \int_{E_o}^{E_c} E^{-\eta} A_{eff}(E,\theta) dE \quad , \tag{4}$$

where (θ,ϕ) are the local coordinates of the bin, ϵ is the efficiency of the bin for detecting source events, ΔT is the burst duration, i.e. T90, A_{eff} is the effective area of the Milagrito detector, which is obtained from Monte Carlo simulations, and which is a function of both primary energy and zenith angle, E_o is the threshold energy for the Milagrito detector, and E_c is an assumed cutoff energy for the GRB flux at the top of the atmosphere. For most GRB search areas, the bin size used was such that $\epsilon \approx 0.5$. The threshold energy of Milagrito for small zenith angles, $\theta \lesssim 25°$, and for a 100-tube trigger requirement, was $E_o \sim 0.3\, TeV$, and increased with increasing zenith angle. N_{90} for a bin with an excess was calculated by using the procedure outlined in Helene (1983). Once N_{90} for each (θ,ϕ) bin with an excess in a GRB search area has been determined, the corresponding flux 90% upper limits on the flux normalizations can be calculated using equation (4). The largest flux upper limit found in a GRB search area was then considered the flux upper limit for that GRB.

Representative 90% upper limits on the flux normalization at 1 TeV for 44 GRBs were determined. Flux upper limits were not determined for all 53 GRBs because some GRB search areas had bins located at zenith angles larger than 60°, for which the effective area of Milagrito could not be easily determined. Assuming a differential spectral index of $\eta = 2.0$, the range of upper limits on the flux normalization at 1 TeV is:

$4 \times 10^{-9} - 10^{-6}$ $\gamma s\ cm^{-2} s^{-1} TeV^{-1}$, with no cutoff at TeV energies;

$4 \times 10^{-8} - 5 \times 10^{-5}$ $\gamma s\ cm^{-2} s^{-1} TeV^{-1}$, with 5-TeV cutoff.

These upper limits as a function of burst duration and zenith angle are plotted in Fig. 4. The

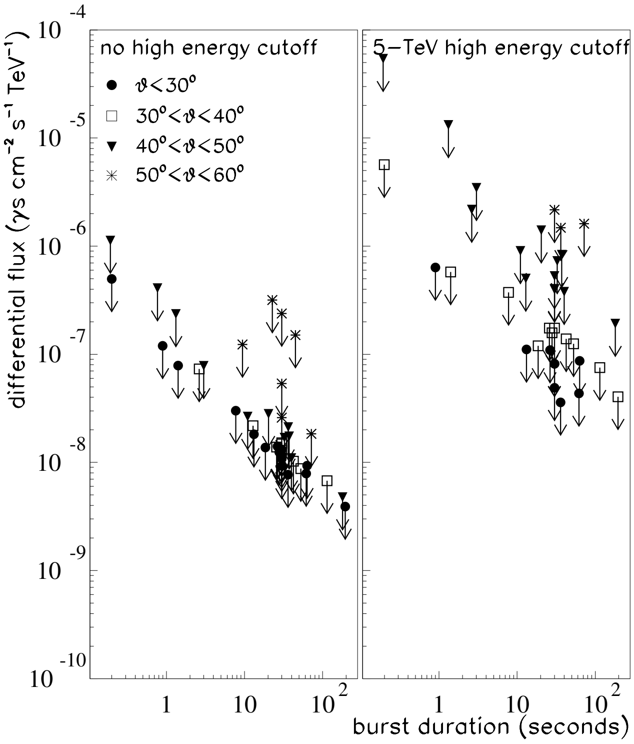

Fig. 4.— 90% upper limits on the flux normalizations at 1 TeV for the GRBs investigated, as a function of burst duration and zenith angle of the bin with the worst (i.e. largest) flux found in a GRB search area. The left panel shows flux limits assuming no spectral cutoff at TeV energies, while the right panel shows flux limits assuming a 5-TeV high energy spectral cutoff. The assumed differential spectral slope was -2.0.

uncertainty in the given flux upper limits, due mainly to the uncertainty in the calculated effective area of Milagrito, A_{eff}, used in equation (4), is about 30% to 40%.

5. Details of Search for GRB 970417a

Table 2 summarizes the parameters for, and results from, the binned search of GRB 970417a for TeV emission. Figures 5 to 8 are plots pertaining to the search results and are explained in the following paragraphs.

Figure 5 shows the spatial distribution of cumulative Poisson probabilities for the occurrence of the on-source counts, or larger, measured in the bins in GRB 970417a's search area. The bin coordinates are given relative to the nominal BATSE position of GRB 970417a, symbolized as (dec0,ra0) in the plot axes. The angular distance between this position ($decl. = 55\overset{\circ}{.}8$, $R.A. = 295\overset{\circ}{.}7$, J2000) and the center of the hottest bin found in the search area ($decl. = 54\overset{\circ}{.}3$, $R.A. = 290\overset{\circ}{.}8$) is $3\overset{\circ}{.}2$. It is also noted that the recently published Stern catalog of BATSE GRBs (Stern et. al. 2001), which was obtained by performing an off-line analysis of the BATSE archival data, has a best fit location for GRB 970417a of $decl. = 54\overset{\circ}{.}2$, $R.A. = 290\overset{\circ}{.}2$, which is an angular distance of only $0\overset{\circ}{.}36$ from the hottest bin found.

Figure 6 shows the spatial distribution of Milagrito events found in the search area of GRB 970417a during the T90 search time interval. Each dot represents a reconstructed air shower event direction, and the ellipses represent the BATSE 68% and 95% confidence ellipses, the latter used as the search area for this GRB analysis. The box is the hottest bin found in the search and contains 17 events. The apparent decrease in the density of events in the (δ, α) plane as the declination increases reflects the fact that to have equal areas on the celestial sphere, over which the density of isotropic background events is constant, the length of the right ascension arc should go as $1/cos(\delta)$, and that, therefore, the density of

Table 2. Parameters for, and results from, GRB 970417a search.

Search Parameter or Measured Quantity	Value
BATSE trigger number	6188
BATSE trigger date[a]	1997 April 17 UT
Beginning of search time interval[b]	13:53:35.6881 UT
BATSE T90[a]	7.936 ± 0.630 seconds
BATSE total fluence ($>$ 20 keV)[a]	$(3.95 \pm 1.94) \times 10^{-7}$ ergs cm^{-2}
BATSE position (J2000)[a]	55°.8 decl., 295°.7 R.A.
Stern catalog position (J2000)[c]	54°.2 decl., 290°.2 R.A.
BATSE 1σ statistical error radius[a]	6°.2
search area (BATSE 95% confidence radius)	11°.4
bin width used in search	2°.851 in decl.
total number of bins used in the search	324
coordinates of center of bin with most significant excess (J2000)	54°.3 decl., 290°.8 R.A.
zenith angle of most significant bin	21°.8
estimated background count in most significant bin	3.41 ± 0.04
on-source count[d] in most significant bin	17
off-source count[d] in most significant bin	9229
on-source to off-source exposure ratio[e]	3.689×10^{-4}
pre-trials cumulative Poisson probability[f] of most significant excess	1.3×10^{-7}
pre-trials significance[f] of most significant excess	5.2 standard deviations
post-trials significance[f] of most significant excess	4.2 standard deviations
final significance[f] of most significant excess	3.2 standard deviations

[a]BATSE data were from the current BATSE Catalog (2000) (http://gammaray.msfc.nasa.gov/batse).

[b]Start of BATSE T90 interval, with a small correction for the difference in arrival times of the signal at BATSE and Milagrito locations.

[c]The Stern catalog can be found in Stern et. al. (2001), and at ftp://ftp.astro.su.se/pub/head/grb/catalogs/etable2.txt.

[d]See Section 3 for definitions.

[e]Ratio of on-source observation time to off-source observation time.

[f]See Section 4 for explanations.

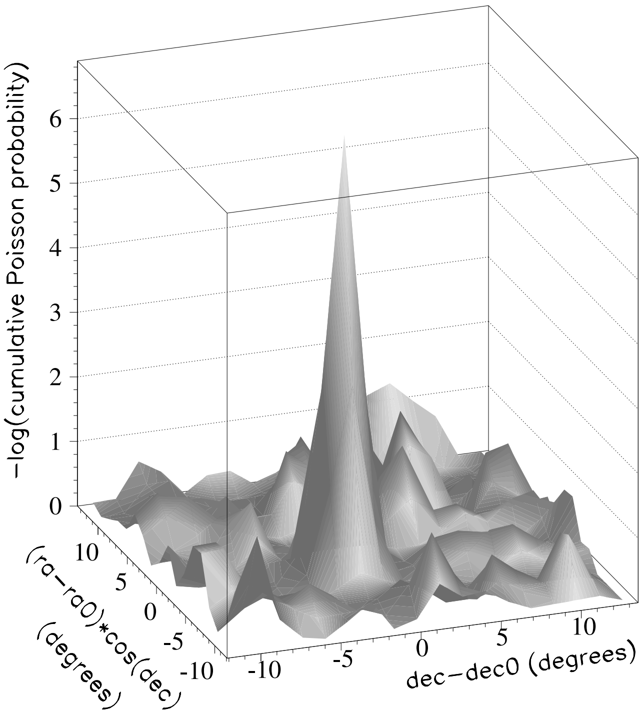

Fig. 5.— Spatial distribution of cumulative Poisson probability in GRB 970417a's search area. The peak corresponds to a probability of 1.3×10^{-7}.

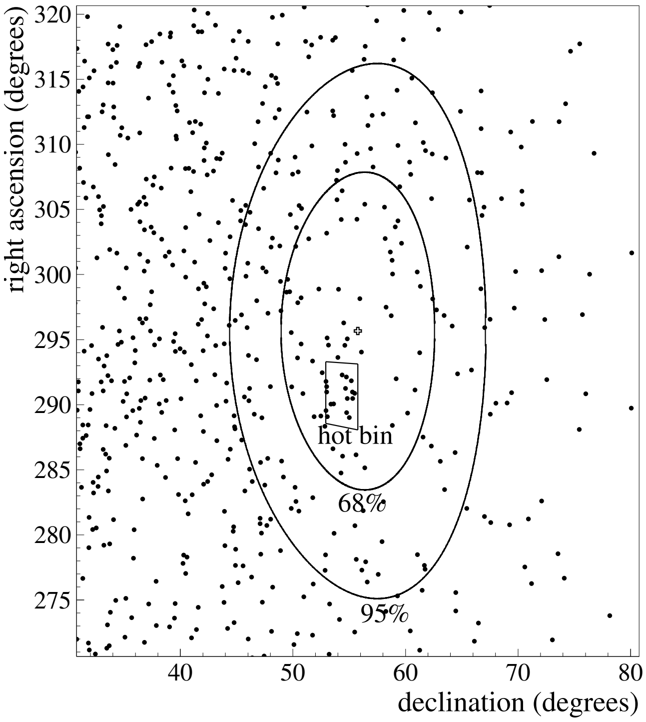

Fig. 6.— Spatial distribution of Milagrito events during the search interval, T90, for GRB 970417a. The ellipses are the BATSE 68% and 95% confidence ellipses for this GRB. The "hot bin" is the bin with the most significant excess found in the search area.

events in the (δ, α) plane goes as $cos(\delta)$.

Figure 7 is the time history of Milagrito events in the local hot bin during six hours surrounding the burst time, i.e. it shows the event count in a local (θ,ϕ) bin over time. It should not be misinterpreted as tracking a source over time, and should not be used to visually search for early or delayed bursts. The time is given relative to the BATSE trigger time for GRB 970417a, and the time bins are each of length T90. The horizontal line is the expected mean background count in the local bin. The on-source count of 17 events is clearly seen coincident with the BATSE trigger.

Figure 8a is a close-up look at the time distribution of Milagrito events in the local hot bin during 30 seconds surrounding the burst time. The time is relative to the BATSE trigger time, and the time bins are each of one second length. Figure 8b is the BATSE count rate for the same time interval. The guide lines delineate the BATSE T90 interval for GRB 970417a.

Aside from the binned analysis, an unbinned maximum likelihood analysis of the air shower events which were in the GRB 970417a search area during T90 was also carried out. In the maximum likelihood analysis, the unknown parameters, namely the celestial coordinates of the source and the number of signal events, were estimated by maximizing the likelihood for the alternative hypothesis, i.e. that a source exists, relative to the likelihood for the null hypothesis, i.e. that no source exists. The random variables used in the analysis were the coordinates of the reconstructed directions of air shower events which were found in the search area during T90. The source was modeled using the average Milagrito point spread function as determined through Monte Carlo simulations. The result of this analysis is shown in Fig. 9, which plots the significance map for the GRB 970417a search area. The maximum likelihood analysis resulted in finding a possible source in the search area, with the estimated source parameters being $decl. = 54\overset{\circ}{.}1$, $R.A. = 290\overset{\circ}{.}9$, and 19.7 signal events.

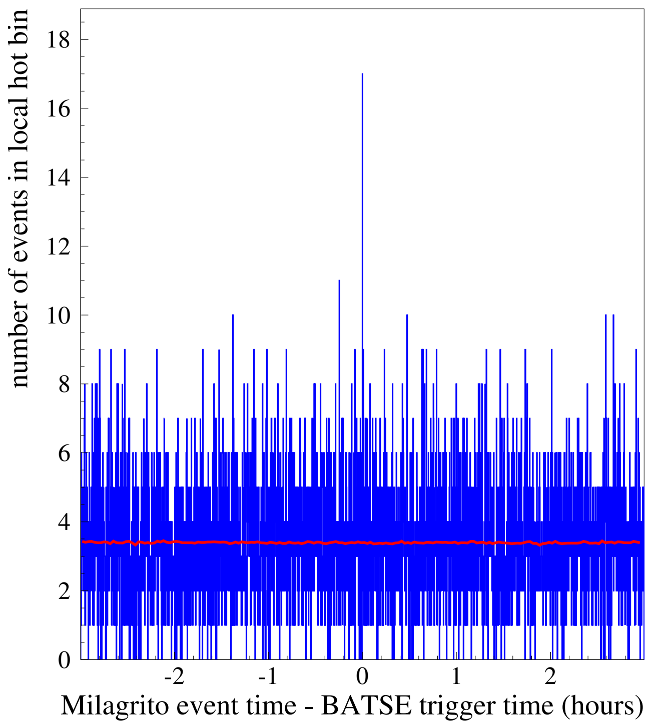

Fig. 7.— Time history of Milagrito events in local hot bin found in GRB 970417a's search area. The horizontal line is the expected background count in the bin.

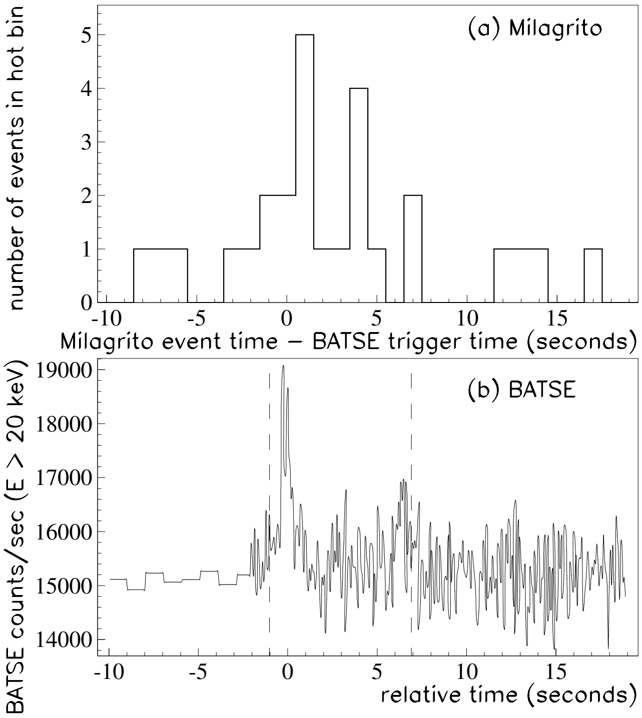

Fig. 8.— (a) Milagrito event time distribution in GRB 970417a hot bin. (b) BATSE event rate for GRB 970417a. The dashed vertical lines delineate the BATSE T90 interval for the GRB. The BATSE light curve data were from The Burst and Transient Source Experiment website (2000), http://cossc.gsfc.nasa.gov/cossc/batse.

The angular distance between the maximum likelihood source position and the center of the bin with the most significant excess in the binned analysis is $0\overset{\circ}{.}21$.

As mentioned in Section 2, as a consequence of the poor core location capability of Milagrito, the experiment did not have the ability to determine the energy of a primary particle which initiated an extensive air shower. Thus, the energies of the primary particles which have been attributed to GRB 970417a are unknown. However, by using the number of PMTs hit by Cherenkov light, produced as a result of an air shower incident on the Milagrito pond, lower limits on the primary particle energies were determined. On the average, an air shower initiated by a primary particle of a certain energy and zenith angle, and whose core lands a certain distance from the pond center, will effect a larger number of tubes hit than will an air shower initiated by a primary with a smaller energy but coming from the same direction, and whose core lands at the same position as that of the first shower core. On the other hand, as it often happens, a small shower whose core lands in the pond can result in a larger number of tubes hit compared to that produced by a big shower whose core lands a great distance from the pond. Knowledge of the real core position is most certainly useful in determining the energy of a primary particle.

The method for placing lower limits on the primary particle energies involved determining a 99.7% confidence upper limit on the number of tubes hit resulting from simulated air showers produced by primary photons of a fixed energy, and coming from a source located at the center of the local hot bin found in GRB 970417a's search area. Since the goal was to determine energy lower limits using the number of tubes hit, and since the nearer a shower core is to the pond the larger the number of tubes hit on the average, the cores of the simulated showers were thrown only within the area defined by the water surface, i.e. 36.6 meters by 56.6 meters. A 1-meter layer of water above the PMTs, the depth at the time of GRB 970417a's activity, was used in the simulations. PMTs which were not used in the actual

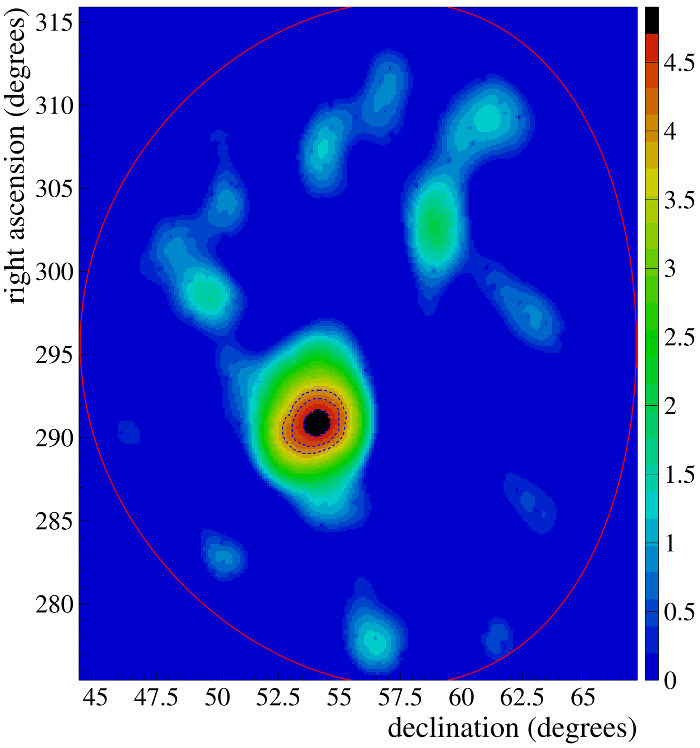

Fig. 9.— Significance map for GRB 970417a's search area, for which the significance was calculated using a maximum likelihood analysis of the air shower events which were in the search area during T90. The colored bar legend on the right of the figure gives the significance corresponding to a certain color. The maximum likelihood estimators for the position of the source are *decl.* = 54.°1, *R.A.* = 290.°9, and the maximum likelihood estimator for the number of signal events is 19.7. The large ellipse is the BATSE 95% confidence ellipse, and the dashed lines are, from smallest to largest, the 68% (bordering the dark spot), 95%, and 99% confidence contours obtained from the maximum likelihood analysis.

reconstructions were not used in the simulations.

The results of the simulations are shown in Figures 10 and 11. Figure 10 is a plot of the distribution of number of tubes hit for different primary photon energies. Figure 11 is obtained from Fig. 10, and plots the ratio of the number of shower events resulting in a given number of tubes or less being hit to the total number of showers thrown, for different primary energies. For a given primary photon energy, the corresponding curve in Fig. 11 gives the probability that an air shower produced by the primary, and whose core lands within the area delineated by the water surface, will result in a given number of tubes or less being hit. Using these results, an upper limit on the number of tubes hit due to primary photons of a given energy, defined as that number of tubes for which the probability for obtaining this number or less is 99.7%, can be determined. The resulting plot of primary photon energy versus upper limit on the number of tubes hit is shown in Fig. 12. This same information is then turned around to obtain a lower limit on the primary photon energy given an observed number of tubes hit. For real air showers whose cores land inside the pond, the energy lower limit obtained through this method will be a 99.7% (3σ) confidence lower limit. For showers with cores landing outside the pond, the energy lower limit obtained through this method will be at a higher confidence level.

Nondetection of a significant excess in the Milagrito scaler counts during T90 (J. McEnery & A. J. Smith 2000, Milagro internal memo) rules out the possibility that the 17 events ascribed to GRB 970417a were due to a large flux of low-energy primary photons or, for that matter, a large flux of any energy. This finding makes reasonable the use of the method outlined above to set lower limits on the primary energies, since ruling out a large photon flux of a certain energy severely limits the occurrence of shower events which give rise to a number of tubes hit which is larger than the upper limit set for that energy.

The lower limits on the primary photon energies corresponding to the detected air

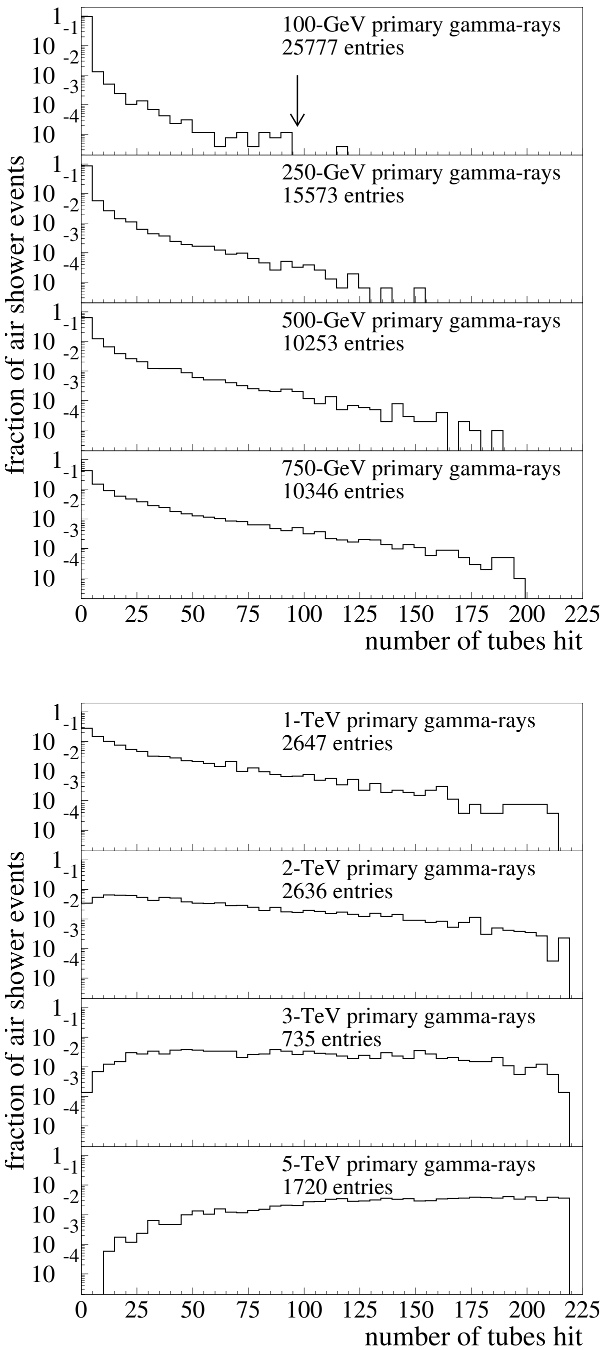

Fig. 10.— Distribution of number of tubes hit for different primary photon energies, obtained using a simulated gamma-ray source located at the center of the local hot bin found in GRB 970417a's search area, and 1 meter of water above the PMTs. The shower cores were thrown over an area defined by the Milagrito water surface. Each distribution is normalized to the number of entries in that distribution. The arrow in the topmost plot marks the number of tubes hit for the detected GRB event resulting in the least number of tubes hit.

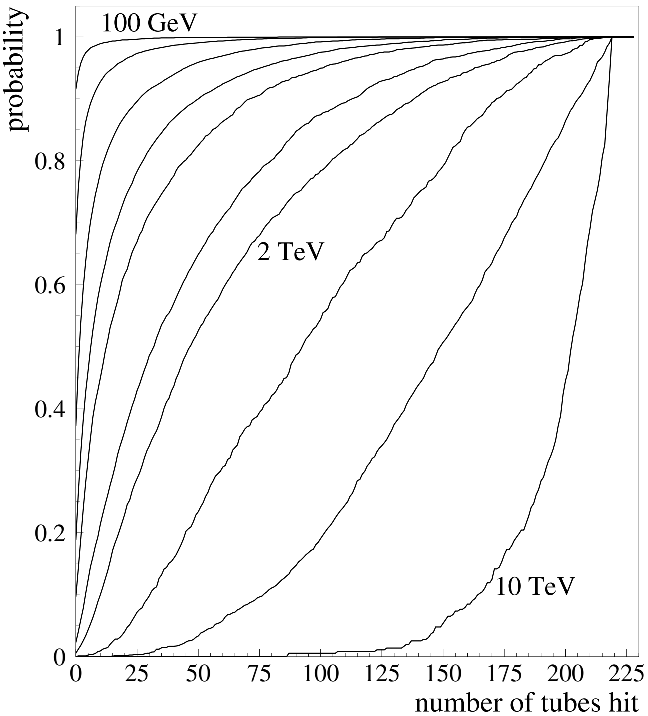

Fig. 11.— Integral distribution of number of tubes hit for different primary photon energies, valid for a source located at the center of the local hot bin found in GRB 970417a's search area, and for 1 meter of water above the PMTs. For a given primary photon energy and a given number of tubes, the corresponding curve gives the probability that an air shower produced by the primary, and whose core lands within the area delineated by the water surface, will result in that number of tubes or smaller being hit. From left to right, the curves correspond to the following primary photon energies: 100 GeV, 250 GeV, 500 GeV, 750 GeV, 1 TeV, 1.5 TeV, 2 TeV, 3 TeV, 5 TeV, and 10 TeV.

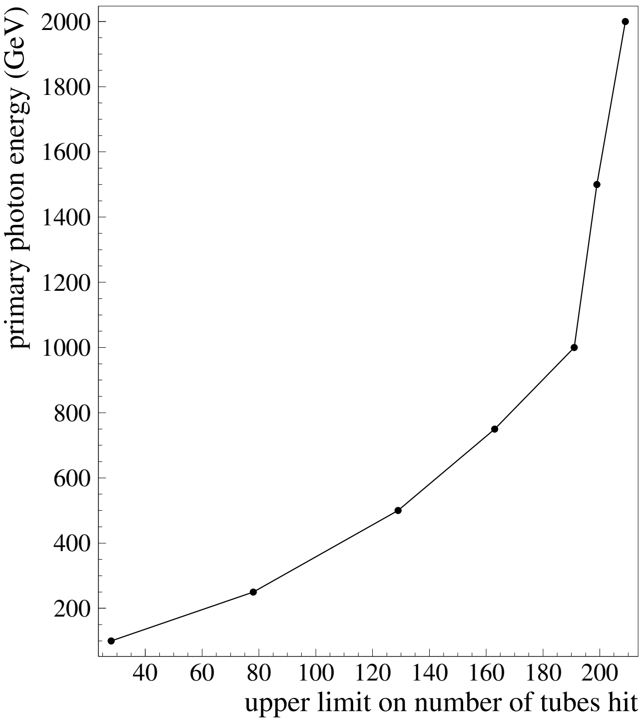

Fig. 12.— Plot of 3σ upper limit on the number of tubes hit for different primary photon energies, derived from Fig. 11. The same plot is used to determine a lower limit on the energy of each of the primary photons initiating the detected air shower events attributed to GRB 970417a, using the observed number of tubes hit for each event.

Table 3. Lower limits on the energies of the detected events.

Event Time (UT seconds)	Relative[a] Event Time (seconds)	Number of Tubes Hit	Energy Lower Limit (GeV)
50015.9980	-0.7155	126	485
50016.3561	-0.3574	171	821
50017.0804	0.3669	175	857
50017.2716	0.5581	143	603
50017.8051	1.0916	105	382
50017.9435	1.2300	143	603
50018.1029	1.3894	161	735
50018.1911	1.4776	129	500
50019.2018	2.4883	97	343
50019.2507	2.5372	114	426
50020.2730	3.5595	139	574
50020.8108	4.0973	102	368
50020.9167	4.2032	125	480
50021.0978	4.3843	167	786
50021.8089	5.0954	111	412
50023.4320	6.7185	169	804
50023.4660	6.7525	182	920

[a]Event time relative to the BATSE trigger time for GRB 970417a.

shower events attributed to GRB 970417a can be found in Table 3. The number of tubes hit for each air shower, and each event's time, are also given. The energy lower limits range from 343 GeV (97 tubes hit) to 920 GeV (182 tubes hit). It is estimated that these energy lower limits are uncertain by about 35%. With these energy lower limits, an upper limit on the fluence of TeV gamma-rays incident at the top of the atmosphere at the time of the burst can be calculated. Using energy lower limits results in an upper limit on the fluence because Milagrito was less sensitive to low-energy photons than to high-energy ones, which means that the total energy incident on Earth due to the GRB has to be concentrated over a smaller area in order for Milagrito to detect low-energy photons. If the energies of the photons were larger than the lower limits, as they might well have been, then the same total incident energy could be spread out over a larger area, that is, the fluence could be lower, and Milagrito would still be able to detect the photons (see Fig. 15 for a plot of fluence, derived from Milagrito's effective area, as a function of primary gamma-ray energy). The fluence upper limit is given by,

$$\Phi_{max} = \sum_{i=1}^{17} \frac{E_{min,i}}{A_{eff,i}} \tag{5}$$

$$= 4.7 \times 10^{-5} \quad ergs\ cm^{-2} \quad , \tag{6}$$

where $E_{min,i}$ is the energy lower limit for a primary event, and $A_{eff,i}$ is the Milagrito effective area for that energy, for a source located at the center of the local hot bin, and for a 1-meter layer of water above the PMTs. The uncertainty in this fluence upper limit is estimated to be about 45%. A fluence of this magnitude is comparable with the largest GRB fluences which have been measured by BATSE.

6. GRB 970417a Distance Scale and Energetics

The probable detection of TeV gamma-rays from GRB 970417a has significant implications on the distance scale and energetics of the GRB. This is so since cosmic TeV gamma-rays, as they travel from the past to the present epoch, are expected to interact with extragalactic background light (EBL) via the electron-positron pair production mechanism. The interaction of TeV photons from an astrophysical gamma-ray source with cosmic background photons results in the attenuation of the TeV photon flux and, consequently, TeV photons originating from very distant epochs, e.g. at redshifts $z \gtrsim 1$, epochs which translate to many pair production interaction lengths, would not be detected by Earth-bound gamma-ray detectors. Detection of TeV photons from a gamma-ray source, thus, would be a strong indication that the source has a small redshift. Two well-studied extragalactic, nearby TeV gamma-ray sources are Mrk 421 ($z = 0.031$) and Mrk 501 ($z = 0.033$). Since GRB 970417a has no known optical counterpart which could have revealed its redshift, examining the opacity of the Universe to TeV photons provides an alternative means for determining the distance scale of the GRB.

Extragalactic background light is diffuse, isotropic radiation originating beyond the Milky Way galaxy, and is a record of the processes which took place during the history of the Universe, including the epoch when rapid star formation in galaxies took place, the epoch when the first stars formed, and the epoch when the Universe first became transparent to radiation produced in the Big Bang. Figure 13 plots the limits and recent detections which have been made of the EBL spectral energy density (SED). The characteristic gamma-ray energies for which the pair production cross section for head-on collissions peaks, given an EBL photon energy or wavelength, are given on the top axis of the figure. For the gamma-ray energies of interest in this work, it is the near to mid infrared component ($\sim 1\ \mu m$ to $\sim 50\ \mu m$) of the EBL SED which is relevant. At present, there is a large uncertainty in the quantitative knowledge about the IR component of the EBL SED, due mainly to difficulties introduced by bright foreground radiation in the task of measuring this component of the EBL SED. This uncertainty is evident in the limits and detections plotted in Fig. 13.

The opacity of the Universe to photons of TeV energies has been estimated by several authors using different models of the EBL SED (Primack et. al. 1999; Stecker & de Jager 1997; Salamon & Stecker 1998; Stecker & de Jager 1998; Dwek & Slavin 1994). For this work, the opacity calculations of Stecker & de Jager (1997) (hereafter SJ97) were adopted. The model EBL SED which these authors used in their calculations is given as a bold, solid line in Fig. 13. The optical depth values calculated by SJ97 using this model are given in Fig. 14, which plots optical depth as a function of observed gamma-ray energy for different source redshifts.

The optical depth, τ, is a measure of the average number of EBL photons which could interact with a TeV photon as the TeV photon makes its way from the past to the present. The larger the optical depth, the lesser the chance the TeV photon has for surviving up to the present epoch. The opacity is thus a function of both the TeV photon energy and the redshift of the source of the TeV photon, $\tau = \tau(E, z_s)$. The probability that a TeV photon of energy E coming from a source redshift z_s will be unabsorbed by the EBL and survive up to the present epoch is given by $exp(-\tau(E, z_s))$. An opacity of unity, for example, would mean a 37% probability of survival. If the differential flux of TeV photons from a gamma-ray source has been measured, then the unattenuated differential flux, corrected for EBL attenuation, would be given by,

$$\left(\frac{dF(E)}{dE}\right)_{unattenuated} = \left(\frac{dF(E)}{dE}\right)_{observed} exp(\tau(E, z_s)) \quad . \tag{7}$$

In the previous section, a lower limit was determined for the energy of each of the 17 primary particles which were detected by Milagrito and ascribed to GRB 970417a. The five largest lower limits obtained ranged from $E \approx 0.8\ TeV$ to $E \approx 0.9\ TeV$ (cf. Table 3).

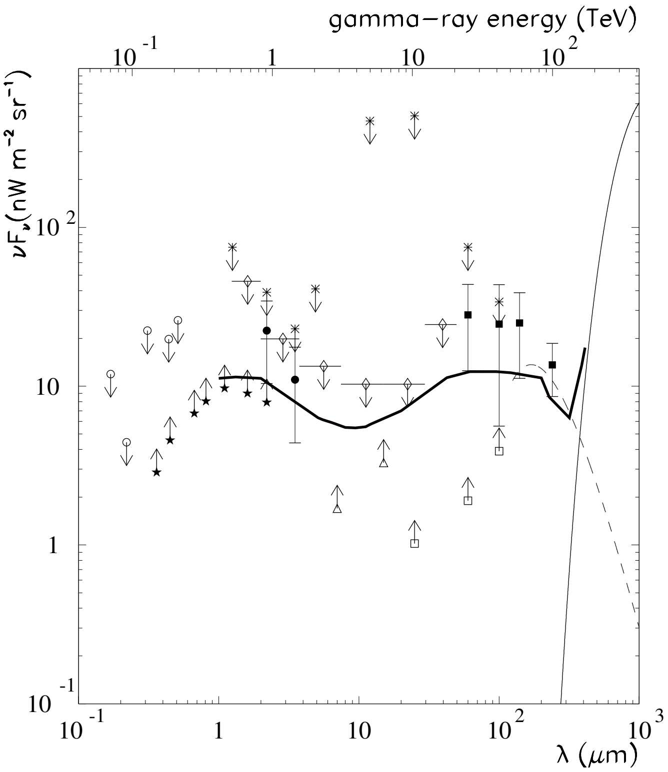

Fig. 13.— Limits on, and detections of, the EBL SED. • and ■ symbols are excesses found in DIRBE data, shown with 2σ error bars (Gorjian, Wright, & Chary 2000; Finkbeiner, Davis, & Schlegel 2000; Hauser et. al. 1998); $*$ symbols are upper limits by DIRBE (Hauser et. al. 1998); $\Diamond$ symbols are upper limits derived by Biller et. al. (1998) from Mrk 421 and Mrk 501 energy spectra; $\circ$ symbols are upper limits from photometry measurements (Maucherat-Joubert, Deharveng, & Cruvellier 1980; Toller 1983; Dube, Wickes, & Wilkinson 1979); ★ symbols are lower limits from Hubble Deep Field and ground-based galaxy counts (Madau & Pozzetti 2000); $\triangle$ symbols are lower limits by ISO (Altieri et. al. 1999); $\Box$ symbols are lower limits by IRAS (Hacking & Soifer 1991). The thin, dashed line is the average EBL SED measured by FIRAS (Fixsen et. al. 1998), and the thin, solid line is the cosmic microwave background spectrum. The thick, solid line is the EBL model used by Stecker & de Jager (1997) for calculating optical depths due to electron-positron pair production.

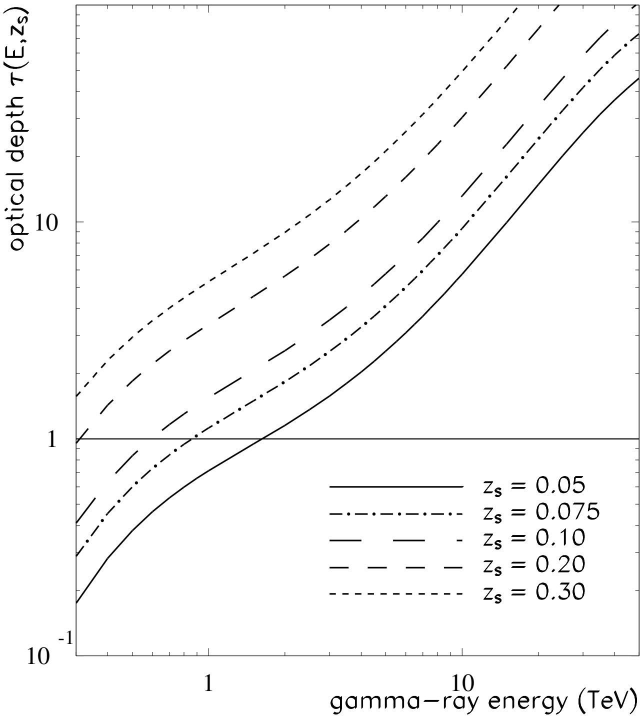

Fig. 14.— Optical depth, calculated by SJ97, due to EBL as a function of gamma-ray energy, for different source redshifts.

Knowledge of these energy lower limits allows the estimate of an upper limit to the distance scale of the GRB. From Fig. 14, it can be seen that gamma-rays with energies $E \approx 0.8\ TeV$ to $E \approx 0.9\ TeV$ have optical depths $\tau \approx 1$, corresponding to a 37% survival probability, if the GRB source redshift is $z_s \lesssim 0.1$. The same conclusion is obtained if the optical depth calculations of Primack et. al. (1999) are used.

The energy lower limits given in Table 3 can also be used to obtain an upper limit on the energy release of GRB 970417a in the TeV waveband, using a justification similar to that used in obtaining an upper limit on the observed GRB fluence (cf. Section 5). The upper limit on the isotropic energy release by GRB 970417a in the TeV regime as a function of GRB redshift is calculated using,

$$E_{iso}(z_s) = \frac{4\pi d_L^2}{1+z_s} \sum_{i=1}^{17} \Phi(E_{min,i})\ exp(\tau(E_{min,i}, z_s)) \quad , \tag{8}$$

where $E_{min,i}$ is the energy lower limit for the i_{th} event, $\Phi(E_{min,i})$ is the fluence at the top of the atmosphere corresponding to this energy, and d_L is the luminosity distance. In terms of Milagrito's effective area, equation (8) is equal to,

$$E_{iso}(z_s) = \frac{4\pi d_L^2}{1+z_s} \sum_{i=1}^{17} \frac{E_{min,i}}{A_{eff,i}}\ exp(\tau(E_{min,i}, z_s)) \quad . \tag{9}$$

Since the effective area of Milagrito for different primary gamma-ray energies is known, it is also possible to set lower limits on the GRB's energy release as a function of redshift, independent of the unknown, actual energy of the highest-energy gamma-ray detected. The basis for determining these lower limits is Fig. 15, which plots the fluence implied by the detection of Milagrito of one primary gamma-ray of a particular energy from the zenith angle of the excess count attributed to GRB 970417a, and for a 1-meter layer of water above the PMTs. The fluence implied by the detection of a photon of energy E is given by $E/A_{eff}(E)$ (in $ergs\ cm^{-2}$). Figure 15 shows that for $E \lesssim 20\ TeV$, the implied fluence decreases as the energy increases. In other words, Milagrito becomes more sensitive as the primary energy

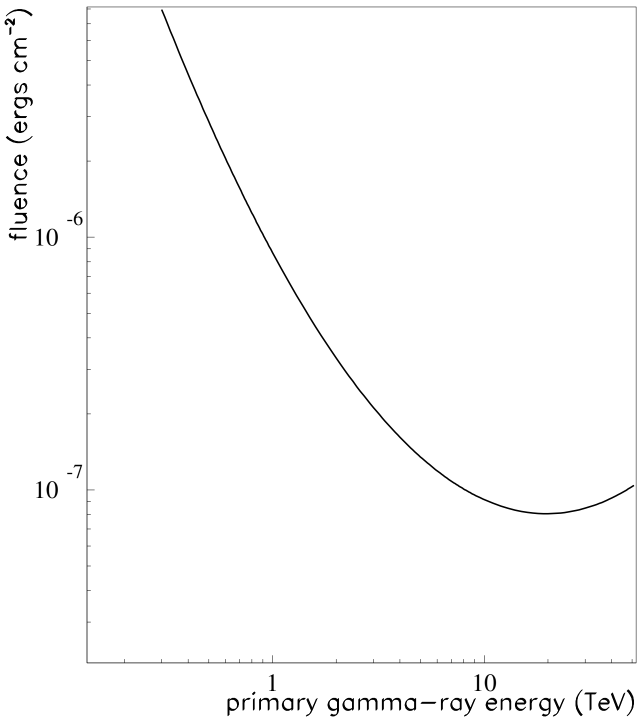

Fig. 15.— Fluence implied by the Milagrito detection of one primary gamma-ray particle of a certain energy, valid for gamma-ray primaries originating from the zenith angle where the excess count attributed to GRB 970417a was found, and for a 1-meter layer of water above the PMTs.

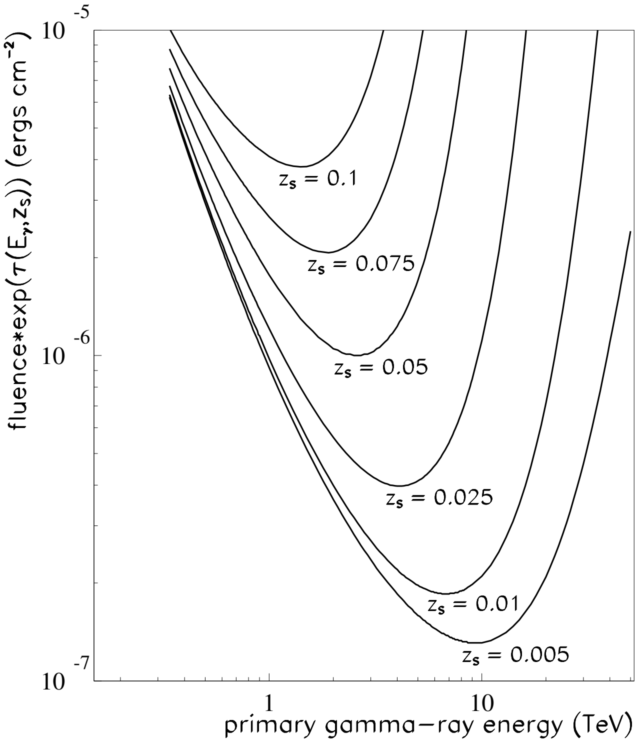

Fig. 16.— Fluence implied by the Milagrito detection of a primary gamma-ray (cf. Fig. 15) after correcting for attenuation by the EBL, assuming different source redshifts, z_s, and using the optical depths of SJ97.

increases because of the corresponding increase in effective area. For $E \gtrsim 20\ TeV$, the effective area does not change very much with increasing primary energy and, thus, the implied fluence increases beyond $E \gtrsim 20\ TeV$. Convoluting this fluence with $exp(\tau(E, z_s))$ to correct for attenuation by the EBL gives Fig. 16, where z_s is an assumed source redshift. It can be seen from Fig. 16 that the curves corresponding to different assumed source redshifts have minimum values. The lower limit on the isotropic energy release of GRB 970417a in the TeV waveband can thus be obtained by using these minimum values in equation (8) for each of the 17 events. Note that the energy release lower limit obtained in this manner is independent of any energy estimates of the primary gamma-ray energies.

Figure 17 plots the upper and lower limits on the energy release by GRB 970417a in the TeV waveband as a function of GRB redshift (bold, solid lines), obtained using the procedure given in the preceding paragraphs. A flat, Einstein-de Sitter Universe with $\Omega_m = 1$, $\Lambda = 0$, and Hubble parameter $H_o = 65\ km\ s^{-1}\ Mpc^{-1}$ were assumed. At the redshift upper limit of $z_s \approx 0.1$, the energy upper and lower limits constrain the energy release to be $E_{iso} \approx 2 \times 10^{51}\ ergs$. Since Fig. 13 suggests that the EBL model used by SJ97 could be at the low side of the actual EBL SED, a check was made on the effect on the energy calculations of doubling the value of the EBL density from the SJ97 model. The resulting effect is shown as short-dashed lines in Fig. 17. As expected, doubling the optical depth lowers the upper limit on the source redshift, but the effect on the energy upper limits is small. Also plotted in Fig. 17 is the implied isotropic energy release at BATSE's waveband (long-dashed line), i.e. using the total fluence measured by BATSE in the soft gamma-ray energy regime. The black dots and the filled star in Fig. 17 give the implied isotropic energy release in the soft gamma-ray waveband for GRBs with known redshifts (cf. Table 1). The open circles give the estimated energy release in soft gamma-rays for five of the GRBs – 990123, 990510, 991216, 000131, and 000301c – if beaming is considered (Kulkarni et. al. 1999; Sari, Piran, & Halpern 1999; Harrison et. al. 1999; Stanek et. al. 1999; Halpern et. al.

2000; Andersen et. al. 2000; Jensen et. al. 2001; Berger et. al. 2000). The filled star is GRB 980425, the GRB which was found spatially and temporally coincident with supernova SN 1998bw (Galama et. al. 1998b; Iwamoto et. al. 1998; Kulkarni et. al. 1998b; Fynbo et. al. 2000), and the open star is GRB 970514, a GRB which has been suggested to be associated with supernova SN 1997cy (Germany et. al. 2000; Turatto et. al. 2000). At a redshift of $z_s \sim 0.01$, the Milagrito lower limit on the isotropic energy release of GRB 970417a is consistent with the estimated isotropic energy release of GRB 980425/SN 1998bw in the soft gamma-ray waveband. Using an alternative cosmology, e.g. with $\Omega_m = 0.3$, $\Omega_\Lambda = 0.7$, is expected to increase these energy estimates by factors of order unity.

7. Summary

Out of 54 BATSE GRBs which were examined for TeV emission, one burst, GRB 970417a, was found to be a candidate for releasing such emission. The event excess found in this GRB's search area had a significance of 5.2 standard deviations, equivalent to a 1.3×10^{-7} cumulative Poisson probability that background fluctuations will give rise to the measured excess count or larger given the expected background. After taking into account all the trials which were used in the search, the final probability for the occurrence of the measured excess due to background fluctuations was found to be 1.4×10^{-3}, or a significance of 3.2 standard deviations. If one considers this final significance, then it is decidedly a marginal excess. On the other hand, closer inspection of the relevant data presented in this work does not reveal any indication that the excess was merely due to a background fluctuation.

Without assuming anything about the unknown spectral shape of the TeV emission from the candidate GRB, and relying a great extent on the fact that the observed events attributed to the candidate GRB could not have been due to a large flux of low-energy primary gamma-rays, it was determined that there was a good probability that the event energies were at

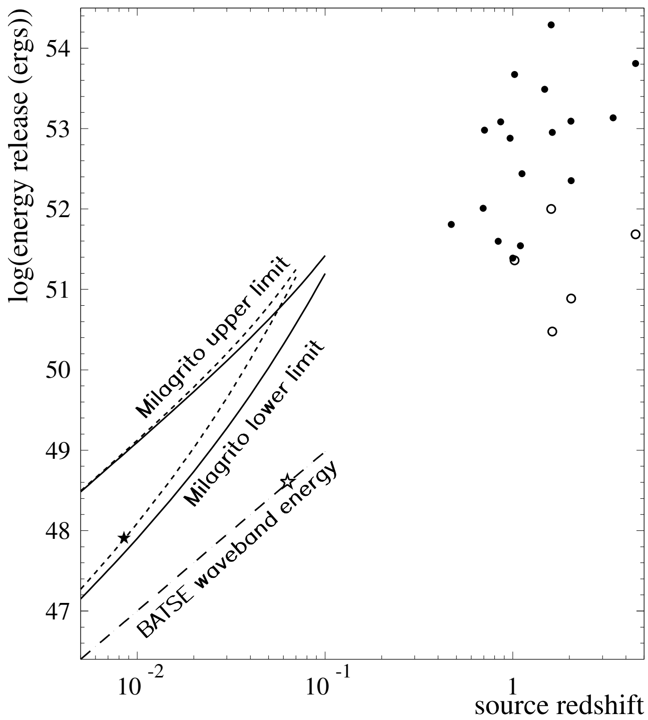

Fig. 17.— Upper and lower limits (thick, solid lines) on the isotropic energy release of GRB 970417a in the TeV waveband, as a function of assumed source redshift, using optical depths of SJ97. The short-dashed lines show the effect on the upper and lower limits of doubling the optical depths from that given by SJ97. The long-dashed line is the energy release of GRB 970417a in soft, keV-MeV gamma-rays, i.e. BATSE's waveband. Also shown are estimates of energy released in the soft gamma-rays by GRBs with known redshifts. The filled circles, filled star, and open star assume isotropic geometry. The open circles show the energy estimates for five of the GRBs when beaming is considered. The filled star is GRB 980425/SN 1998bw, and the open star is GRB 970514/SN 1997cy. A cosmology with $\Omega_m = 1$, $\Lambda = 0$, and $H_o = 65\ km\ s^{-1}\ Mpc^{-1}$ was assumed for all of the energy calculations.

least in the energy range of ~ 0.3 to ~ 1 TeV, and that the event energies could be larger than this range. Consideration of the interaction of extragalactic photons of TeV energies with the cosmic infrared background radiation puts an upper limit of $z \sim 0.1$ on the distance scale of the candidate GRB. This places the candidate GRB among the closest GRBs found, given that the median redshift of the GRBs with well-established redshifts is $z \approx 1$. It is noted that the redshifts of the GRBs which have been suggested to have originated "nearby", i.e. GRB 980425/SN 1998bw, GRB 970514/SN 1997cy, have not attained the same secure status as the well-established redshifts of "cosmological" GRBs, due to the fact that the disputed redshifts were obtained by temporally and spatially associating the GRBs with observed supernovae. But if the distribution of GRBs traces the star formation history of the Universe, then it is expected that a small fraction of GRBs would be found at $z \ll 1$, and the detection of nearby GRBs would be consistent with the true spatial distribution of GRBs.

Due to the unknown distance to the candidate GRB, the implied isotropic energy release in the TeV waveband is hard to establish. An estimate of the isotropic energy release in the TeV waveband ranges from $E_{iso} \sim 2 \times 10^{51}$ $ergs$ at $z \approx 0.1$, which is consistent with the derived energy release in the keV-MeV waveband by GRBs at $z \sim 1$, to $E_{iso} \sim 2 \times 10^{47}$ $ergs$ at $z \approx 0.005$, which is consistent with the implied energy release of GRB 980425/SN 1998bw. A comparison of these energy estimates in the TeV waveband with the implied isotropic energy release of GRB 970417a in the keV-MeV waveband strongly suggests that if GRB 970417a emitted TeV radiation, then most of the energy released in the gamma-ray burst was in the form of TeV photons. In this case, a small measured flux or fluence in the keV-MeV energy range would not mean that the GRB is far and therefore results in a weak signal on Earth, as is usually assumed in modelling the GRB spatial distribution, but that most of the energy is found at the TeV waveband.

The results presented in this work do not provide an unequivocal answer to the question of the actuality of a TeV component of GRBs, and perhaps the final judgement on this scientific work will be provided in retrospect. Pinning down the elusive answer to this question is the current and future task of TeV gamma-ray detectors, one of which is Milagro, a more sensitive analogue of Milagrito, and which has been in operation since February 1999. A convincing detection of a TeV component of GRBs is one way to confirm the presence of highly relativistic electrons in GRBs and, thus, to validate the relativistic fireball model of GRBs.

The authors would like to acknowledge the technical support and indispensable contributions of Scott Delay, Michael Schneider, and Neil Thompson to the experiment. We also thank the BATSE Collaboration for doing a great job and for making their data easily accessible through the Internet. This work was supported by the National Science Foundation, the US Department of Energy Offices of High Energy Physics and Nuclear Physics, the Los Alamos National Laboratory, the University of California, and the Institute of Geophysics and Planetary Physics.

REFERENCES

Aglietta, M., et. al. 1996, ApJ, 469, 305

Aharonian, F. A., et. al. 1999a, A&A, 342, 69

Aharonian, F., et. al. 1999b, A&A, 349, 29

Aharonian, F. A., et. al. 2000, ApJ, 539, 317

Alexandreas, D. E., et. al. 1994, ApJ, 426, L1

Altieri, B., et. al. 1999, A&A, 343, L65

Amati, L., et. al. 2000, Science, 290, 953

Amenomori, M., et. al. 1996, A&A, 311, 919

Andersen, M. I., et. al. 2000, A&A, 364, L54

Antonelli, L. A., et. al. 2000, ApJ, 545, L39

Atkins, R., et. al. 2000a, ApJ, 533, L119

Atkins, R., et. al. 2000b, Nucl. Instr. Meth. Phys. Res. A, 449, 478

BATSE Catalog, Burst and Transient Source Experiment, 2000, http://gammaray.msfc.nasa.gov/batse

Berger, E., et. al. 2000, ApJ, 545, 56

Biller, S. D., et. al. 1998, Phys. Rev. Lett., 80, 2992

Bloom, J. S., Djorgovski, S. G., Kulkarni, S. R., & Frail, D. A. 1998, ApJ, 507, L25

Bloom, J. S., et. al. 1999a, Nature, 401, 453

Bloom, J. S., Sigurdsson, S., & Pols, O. R. 1999b, MNRAS, 305, 763

Bloom, J. S., Djorgovski, S. G., & Kulkarni, S. R. 2000a, ApJ, in press (astro-ph/0007244)

Bloom, J. S., et. al. 2000b, GCN Circ. 661

Bloom, S. D., & Marscher, A. P. 1996, ApJ, 461, 657

Boella, G., Butler, R. C., Perola, G. C., Piro, L., Scarsi, L., & Bleeker, J. A. M. 1997, A&AS, 122, 299

Bradt, H. V., & Smith, D. A. 1999, A&AS, 138, 423

Briggs, M. S., Pendleton, G. N., Kippen, R. M., Brainerd, J. J., Hurley, K., Connaughton, V., & Meegan, C. A. 1999, ApJS, 122, 503

Castro, S. M., et. al. 2000, GCN Circ. 851

Connaughton, V., et. al. 1997, ApJ, 479, 859

Costa, E., et. al. 1997, Nature, 387, 783

de Jager, O. C., & Harding, A. K. 1992, ApJ, 396, 161

de Jager, O. C., Harding, A. K., Michelson, P. F., Nel, H. I., Nolan, P. L., Sreekumar, P., & Thompson, D.J. 1996, ApJ, 457, 253

Djorgovski, S. G., Kulkarni, S. R., Bloom, J. S., Goodrich, R., Frail, D. A., Piro, L., & Palazzi, E. 1998, ApJ, 508, L17

Djorgovski, S. G., Bloom, J. S., & Kulkarni, S. R. 2000, ApJL, submitted (astro-ph/0008029)

Dodonov, S. N., Afanasiev, V. L., Sokolov, V. V., Moiseev, A. V., & Castro-Tirado, A. J. 1999, GCN Circ. 475

Dube, R. R., Wickes, W. C., & Wilkinson, D. T. 1979, ApJ, 232, 333

Dwek, E., & Slavin, J. 1994, ApJ, 436, 696

Finkbeiner, D. P., Davis, M., & Schlegel, D. J. 2000, ApJ, 544, 81

Fishman, G. J. 1992, in Gamma-Ray Bursts, Proceedings of the Los Alamos Workshop on Gamma-Ray Bursts, ed. C. Ho, R. I. Epstein, & E. E. Fenimore (Cambridge: Cambridge University Press) 265

Fixsen, D. J., Dwek, E., Mather, J. C., Bennett, C. L., & Shafer, R. A. 1998, ApJ, 508, 123

Fynbo, J. U., et. al. 2000, ApJ, 542, L89

Galama, T. J., et. al. 1998a, ApJ, 497, L13

Galama, T. J., et. al. 1998b, Nature, 395, 670

Germany, L. M., Reiss, D. J., Sadler, E. M., Schmidt, B. P., & Stubbs, C. W. 2000, ApJ, 533, 320

Gorjian, V., Wright, E. L., & Chary, R. R. 2000, ApJ, 536, 550

Greiner, J. 2000, Table of well-localized GRBs, http://www.aip.de/~jcg/grbgen.html

Groot, P. J., et. al. 1998, ApJ, 502, L123

Hacking, P. B., & Soifer, B. T. 1991, ApJ, 367, L49

Halpern, J. P., et. al. 2000, ApJ, 543, 697

Harrison, F. A., et. al. 1999, ApJ, 523, L121

Hauser, M. G., et. al. 1998, ApJ, 508, 25

Helene, O. 1983, Nucl. Instr. Meth., 212, 319

Hillas, A. M., et. al. 1998, ApJ, 503, 744

Hjorth, J., Holland, S., Courbin, F., Dar, A., Olsen, L. F., & Scodeggio, M. 2000, ApJ, 534, L147

Hogg, D. W., & Fruchter, A. S. 1999, ApJ, 520, 54

Hurley, K. 1999, A&AS, 138, 553

Hurley, K., et. al. 2000a, ApJ, 534, L23

Hurley, K., et. al. 2000b, GCN Circ. 801

Hurley, K., et. al. 2000c, GCN Circ. 802

In 't Zand, J. J. M., et. al. 2001, ApJL, submitted (astro-ph/0104362)

Inoue, S., & Takahara, F. 1996, ApJ, 463, 555

Iwamoto, K., et. al. 1998, Nature, 395, 672

Jensen, B. L., et. al. 2001, A&A, in press (astro-ph/0005609)

Jha, S., et. al. 2001, ApJL, accepted (astro-ph/0103081)

Klose, S., et. al. 2000, ApJ, 545, 271

Krennrich, F., et. al. 1997, ApJ, 481, 758

Krennrich, F., et. al. 1999, ApJ, 511, 149

Kulkarni, S. R., et. al. 1998a, Nature, 393, 35

Kulkarni, S. R., et. al. 1998b, Nature, 395, 663

Kulkarni, S. R., et. al. 1999, Nature, 398, 389

Lamb, D. Q. 2000, Phys. Rep., 333-334, 505

Lamb, D. Q., & Reichart, D. E. 2000, ApJ, 536, 1

Levine, A. M., Bradt, H., Cui, W., Jernigan, J. G., Morgan, E. H., Remillard, R., Shirey, R. E., & Smith, D. A. 1996, ApJ, 469, L33

Li, T.-P., & Ma, Y.-Q. 1983, ApJ, 272, 317

MacFadyen, A. I., & Woosley, S. E. 1999, ApJ, 524, 262

Madau, P., & Pozzetti, L. 2000, MNRAS, 312, L9

Maraschi, L., et. al. 1999, ApJ, 526, L81

Maucherat-Joubert, M., Deharveng, J. M., & Cruvellier, P. 1980, A&A, 88, 323

Metzger, M. R., Djorgovski, S. G., Steidel, C. C., Kulkarni, S. R., Adelberger, K. L., & Frail, D. A. 1997a, IAU Circ. 6655

Metzger, M. R., Cohen, J. G., Chaffee, F. H., & Blandford, R. D. 1997b, IAU Circ. 6676

Paczyński, B. 1998, ApJ, 494, L45

Padilla, L., et. al. 1998, A&A, 337, 43

Pendleton, G. N., et. al. 1999, ApJ, 512, 362

Petry, D., et. al. 2000, ApJ, 536, 742

Pilla, R. P., & Loeb, A. 1998, ApJ, 494, L167

Piran, T. 1999, Phys. Rep., 314, 575

Piran, T. 2000, Phys. Rep., 333-334, 529

Primack, J. R., Bullock, J. S., Somerville, R. S., & MacMinn, D. 1999, Astropart. Phys., 11, 93

Quinn, J., et. al. 1999, ApJ, 518, 693

Rosswog, S., Liebendörfer, M., Thielemann, F.-K., Davies, M. B., Benz, W., & Piran, T. 1999, A&A, 341, 499

Ruffert, M., & Janka, H.-Th. 1999, A&A, 344, 573

Sahu, K. C., et. al. 2000, ApJ, 540, 74

Salamon, M. H., & Stecker, F. W. 1998, ApJ, 493, 547

Samuelson, F. W., et. al. 1998, ApJ, 501, L17

Sari, R., Piran, T., & Halpern, J. P. 1999, ApJ, 519, L17

Stanek, K. Z., Garnavich, P. M., Kaluzny, J., Pych, W., & Thompson, I. 1999, ApJ, 522, L39

Stecker, F. W., & de Jager, O. C. 1997, ApJ, 476, 712

Stecker, F.W., & de Jager, O.C. 1998, A&A, 334, L85

Stern, B. E., Tikhomirova, Y., Kompaneets, D., Svensson, R., & Poutanen, J. 2001, ApJ, in press (astro-ph/0009447)

Takahashi, T., et. al. 2000, ApJ, 542, L105

Tanimori, T., et. al. 1998, ApJ, 492, L33

Toller, G. N. 1983, ApJ, 266, L79

Totani, T. 1999, ApJ, 511, 41

Turatto, M., et. al. 2000, ApJ, 534, L57

van Paradijs, J., et. al. 1997, Nature, 386, 686

Vietri, M., & Stella, L. 1998, ApJ, 507, L45

Vreeswijk, P. M., et. al. 1999, ApJ, 523, 171

Wijers, R. A. M. J., Bloom, J. S., Bagla, J. S., & Natarajan, P. 1998, MNRAS, 294, L13

Wijers, R. A. M. J., et. al. 1999, ApJ, 523, L33

Woods, P., et. al. 1998, GCN Circ. 112

Woosley, S. E. 1993, ApJ, 405, 273

Woosley, S. E., & MacFadyen, A. I. 1999, A&AS, 138, 499

Zweerink, J. A., et. al. 1997, ApJ, 490, L141
